



## The 94-GHz radar dim band: Relevance to ice cloud properties and CloudSat

Andrew J. Heymsfield,<sup>1</sup> Aaron Bansemer,<sup>1</sup> Sergey Matrosov,<sup>2</sup> and Lin Tian<sup>3</sup>

Received 26 July 2007; revised 23 October 2007; accepted 23 November 2007; published 1 February 2008.

[1] Details of the microphysics are shown to be responsible for a region of ice cloud which, when probed from above, has decreasing radar reflectivity ( $Z_e$ ) downwards at 94 GHz but increasing  $Z_e$  at 9.7 GHz. This 94-GHz radar dim band is found to be due to the combination of ice particle aggregation and non-Rayleigh scattering effects. Observations and model calculations indicate that it occurs when the particle size distribution (PSD) broadens such that its slope, as derived from fitted PSD, decreases below about  $15 \text{ cm}^{-1}$ , or equivalently, to a median volume diameter exceeding 0.25 cm. Dimming occurs at temperatures ( $T$ ) primarily between  $-5$  and  $0^\circ\text{C}$  but can occur at  $-30^\circ\text{C}$  or below in convectively-generated ice clouds (anvils). The dimming effect may produce an appreciable low bias in the ice water content (IWC) retrieved from  $Z_e$  measured by CloudSat's 94-GHz radar. Methods to estimate the IWC in the dim band are proposed. **Citation:** Heymsfield, A. J., A. Bansemer, S. Matrosov, and L. Tian (2008), The 94-GHz radar dim band: Relevance to ice cloud properties and CloudSat, *Geophys. Res. Lett.*, 35, L03802, doi:10.1029/2007GL031361.

### 1. Introduction

[2] CloudSat, with an onboard 3.2 millimeter wavelength (94 GHz) W-band radar, presents a new opportunity to characterize the microphysical properties of ice clouds on a global scale for evaluating and improving the representation of clouds in climate models [Stephens *et al.*, 2002]. To achieve this goal, it is necessary to explain distinctive features found in the remote sensing of ice particle populations with a W band radar. The goal of this article is to provide an explanation for one such W-band feature.

[3] Stratiform cloud layers with precipitation-size particles often have three radar-discernible layers: an ice-phase region for  $T \leq 0^\circ\text{C}$ , a melting layer (ML), with large melting ice near the top and raindrops near the bottom; and rain below. Particles in the ice regions can develop to sizes of 1 cm or beyond through aggregation, especially for  $-10 < T \leq 0^\circ\text{C}$  (Heymsfield *et al.* [2002], hereafter H02, and others). Large aggregates falling within the ML often produce a bright band for X band (e.g., 9.7 GHz) radars. However, measurements from a W band radar are influenced by non-Rayleigh scattering effects within the ML because cm-size particles are large compared to the radar's wavelength. Because of attenuation and non-Rayleigh scat-

tering, W band  $Z_e$  profiles through the ML are usually flat [Kollias and Albrecht, 2005; Sassen *et al.*, 2005, 2007].

[4] This study is concerned with characterizing and explaining 94-GHz radar observations when large, dry ice particles are present. A curious finding in the vertically pointing W-band radar observations of Lhermitte [1988] is the reduction in the radar reflectivity,  $Z_e$ , of almost 10 dB in a layer beginning from about 1 km above the ML to the top of the ML; the ML height is ascertained from an abrupt increase in the mean Doppler fallspeed,  $V_z$ . Kollias and Albrecht [2005] note that at 94 GHz, there is often, at low rainfall rates, a small decrease of 1 or 2 dB in  $Z_e$  observed just above the  $0^\circ\text{C}$  isotherm. In the study of Sassen *et al.* [2005] (hereafter S05) which uses three upward-pointing Doppler radars operating at different frequencies,  $Z_e$  for X band increases down to the ML whereas for W band it is nearly constant.

[5] This "dim" band can be identified from above, without intervening attenuation by rain or melting ice, in data collected by the nadir-pointing Doppler radars on board the NASA ER-2, EDOP (9.7 GHz) and CRS (94 GHz) [Tian *et al.*, 2007]. These radars profiled a stratiform cloud layer over southern Florida on 11 July 2002 during the Cirrus Regional Study of Tropical Anvils and Cirrus Layers Florida Area Cirrus Experiment (CRYSTAL- FACE, hereinafter C-F). The cloud and period studied, from 19.18 to 19.32 UTC, coincided with the study by S05. Temperatures and GPS altitudes were derived from in-situ aircraft measurements and ER-2 dropsondes to convert radar height to temperature, with the  $0^\circ\text{C}$  level at 4.68 km MSL.

[6] Of the 150 consecutive EDOP and CRS radar profiles examined during this period, all but two showed a decrease in  $Z_e$  of up to 4 dBZ at 94 GHz but a corresponding increase of several dBZ at 9.7 GHz (Figure 1). At the top of the dim band,  $Z_e$  (94 GHz) =  $6.4 \pm 0.6$  dB. The  $V_z$  in the layer are about  $200 \text{ cm s}^{-1}$  for  $-10 < T \leq 0^\circ\text{C}$ , signifying  $Z_e$  is dominated by aggregates (H02). The ML, with increased  $V_z$ , lies below the dim band. Attenuation from cloud top downwards only accounts for several tenths of a dB decrease in  $Z_e$  at 94 GHz (discussed later).

[7] The measurements and methods used to examine the dim band are given in section 2 and the observations and the results of calculations used to quantify the dimming effect are presented in section 3. The main findings are summarized in section 4.

### 2. Methods

[8] A mixture of Rayleigh and non-Rayleigh scattering occur at W-band wavelengths. Figure 2 shows the backscatter cross-sections,  $\sigma$ , at 94 GHz for spherical particles to simulate complex, 3-D ice shapes, and for oblate (0.6:1

<sup>1</sup>National Center for Atmospheric Research, Boulder, Colorado, USA.

<sup>2</sup>Environmental Technology Laboratory, NOAA, Boulder, Colorado, USA.

<sup>3</sup>NASA Goddard Space Flight Center, Greenbelt, Maryland, USA.

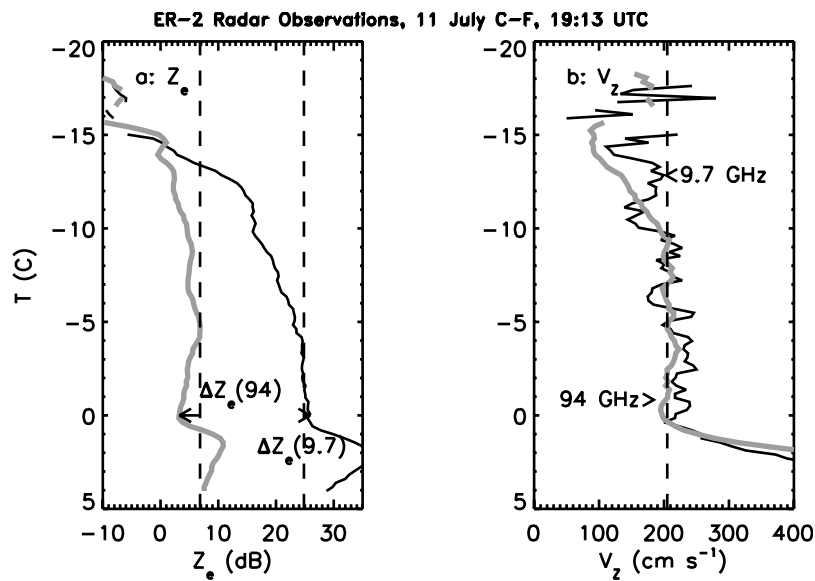


**Figure 1.** Profiles of radar reflectivities and Doppler velocities from ER-2 radars pointing nadir on 11 July 2002 at 19:22 UTC hrs. Heights are converted to temperatures from aircraft soundings.

axial ratio) ones to simulate aggregates with their minor axis oriented vertically. They are derived using the T-matrix approach discussed by *Matrosov et al.* [2005], with particle densities varying as  $D^{-1.1}$  as discussed later in this section. There is a six-fold higher peak cross-section for oblate than spherical particles. The  $\sigma$  deviate from Rayleigh scattering—the highlighted portion of the curve for oblate particles at 94 GHz—, when the maximum particle diameter,  $D$ , is above about 0.12 cm. At 9.7 GHz, the deviation occurs when  $D$  is about ten times larger. The fitted relationships for  $\sigma(D)$  are also shown in Figure 2 in the Rayleigh regime. Peak and minimum values of  $\sigma$  in the non-Rayleigh regime at 94 GHz are relatively constant for  $0.15 < D < 2$  cm, largely due to the assumed decrease in density,  $\rho \propto D^{-1.1}$ , with size. Significant non-Rayleigh effects are noted at 94 GHz for other  $\rho(D)$  relationships that produce accurate IWC's ( $\rho = f(D^{-0.9})$ , Figure 2).

[9] The backscattering cross sections from Figure 2 are used to calculate  $Z_e$  at 94 and 9.7 GHz from the PSD measured during Lagrangian spiral descents through deep, convectively-generated ice cloud layers (anvils) sampled by the University of North Dakota Citation. Data from spirals on nine days during the Kwajalein Experiment (KWAJEX) in the Marshall Islands in 1999 and from the C-F project in southern Florida in 2002 are examined. Sampling was conducted throughout the range  $-50 < T \leq 0^\circ\text{C}$ . PSD from 50 or 100  $\mu\text{m}$  to above 2 cm were measured from two 2D imaging probes (see H02) and binned into 33 sizes. Averaging times were 5-sec. or about 0.6 km of flight path. Exponential curves,  $N = N_0 e^{-\lambda D}$ , where  $N$  is the normalized ice concentration,  $N_0$  the intercept parameter, and  $\lambda$  the slope, have been fitted to each of the PSD (see H02). A total of more than 3000, 5-sec data points were acquired during the spirals.

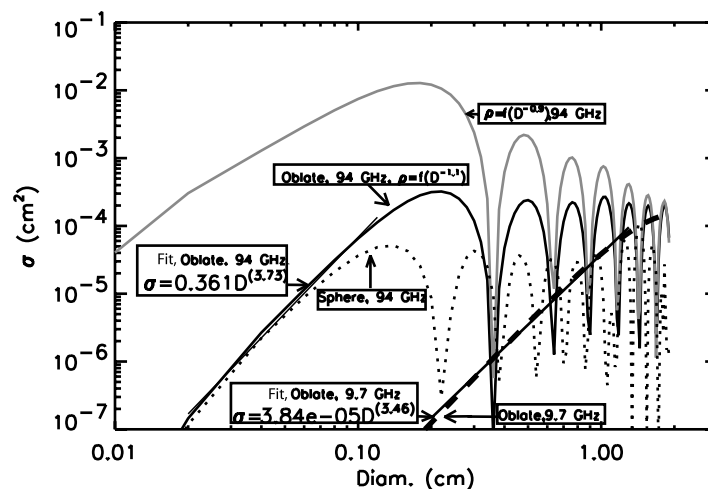


**Figure 2.** Backscatter cross sections derived from the T-matrix method discussed by *Matrosov et al.* [2005] for spherical and oblate ice particles for radar frequencies of 94 and 9.7 GHz. The diameters are the maximum particle dimension and for a given  $D$ , the masses of spherical and nonspherical particles are the same.

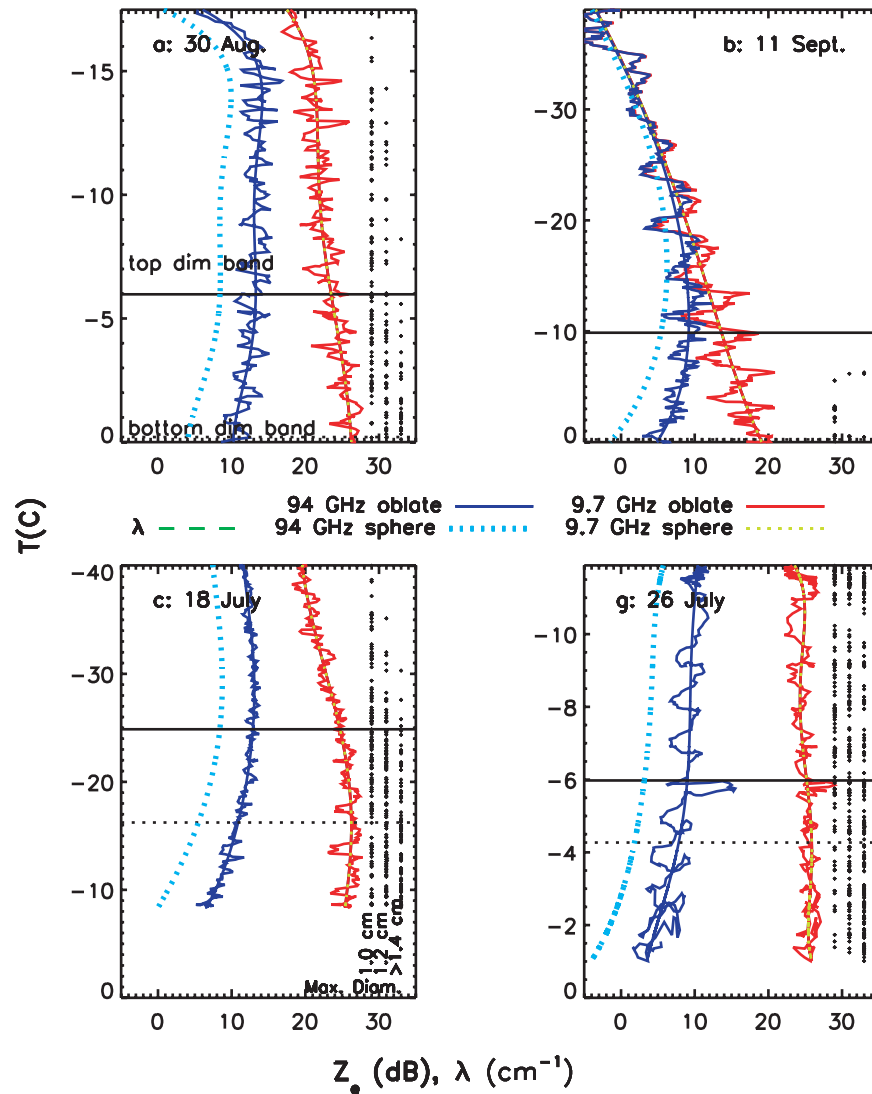


**Figure 3.** Calculated radar reflectivities at two radar frequencies for oblate ice particles with a 0.6 to 1 axial ratio and assuming spherical ice particles with an axial ratio of 0.6 to 1 using the measured PSD and  $m(D)$  relationship (see text). (a, b) KWAJEX field campaign. (c, d) CRYSTAL-FACE. Fifth order polynomial curves are fitted to the  $Z_e$  profiles for the oblate particles to allow the trends in the vertical to be more readily discerned. Regions where the maximum diameter for each PSD exceeds 1 cm, 1.2, and 1.4 cm are indicated by dots in three columns on the right side of each plot. Profiles of the slopes of the exponential fits to the PSDs are shown.

[10] The IWC was measured directly during C-F. The IWC is also calculated using the PSD together with a mass ( $m$ ) dimensional relationship,  $m(\text{g}) = a[D(\text{cm})]^b$ . Brown and Francis [1995] (hereafter BF95), and Heymsfield *et al.* [2007] (hereafter H07) report that  $b \approx 1.9$ . The  $a$  coefficient is taken to be  $0.00469 (\text{g cm}^{-1.9})$ , which is 60% larger than  $a$  given by BF95 but essentially the same as given by H07. For the C-F clouds, the ratio of the IWC calculated from the PSD to the measured values is excellent overall:  $1.06 \pm 0.4$  for  $\text{IWC} > 0.1 \text{ g m}^{-3}$ ; these IWC dominate the dim band.

### 3. Results

[11] Figure 3 compares calculated profiles of  $Z_e$  at 94 and 9.7 GHz from four spirals. Non-Rayleigh effects are more pronounced for spherical than oblate particles of the same masses, resulting in  $Z_e$  for spherical particles that are several dB lower than for the oblate ones.

[12] Polynomial curves are fitted to the calculated  $Z_e$  profiles for the oblate particles in Figure 3 to damp out fluctuations due to horizontal variability along the 10 km or so diameter paths of the spirals. This procedure adds clarity to the trends in the vertical and allows us to define tops and bottoms of the dim bands: where there is a decrease in  $Z_e$  for 94 GHz and an increase in  $Z_e$  at 9.7 GHz. Each cloud in Figure 3 has dim bands. The bottom of the band did not reach the  $0^\circ\text{C}$  level on 18 July (C-F, Figure 3c) and 22 July (KWAJEX, not shown). Significant sublimation in the lower levels of these clouds washes out this band. The dim band is relatively insensitive to the choice of  $b$  in the  $m(D)$  relationship, provided that the calculated IWC reproduce the measured ones; with  $b = 2.1$  (Figure 2), the dimming is about 2 dB larger.

[13] PSD characteristics, namely the maximum particle diameter,  $D_{\text{max}}$ , and the slope  $\lambda$ , are also shown in Figure 3.

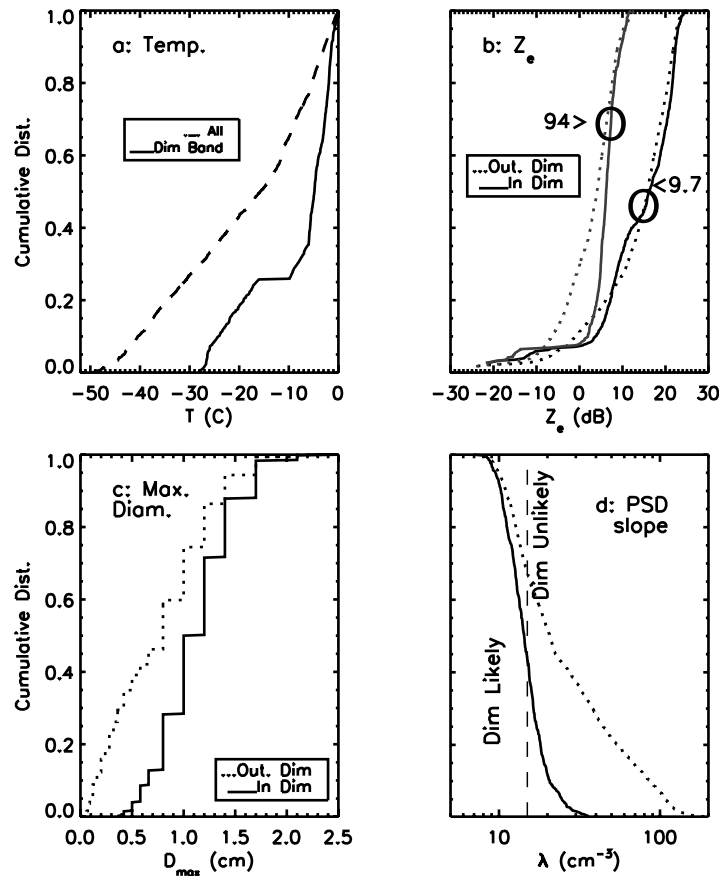


**Figure 4.** Summary of results from 9 Lagrangian spiral descents through ice cloud layers, separated by whether within or outside of the dim band. (a) Cumulative probability distribution of temperatures measured, shown for all 5-sec periods. (b)  $Z_e$  at two wavelengths. (c) Maximum diameter. (d) Slope of the PSD.

The  $D_{\max}$  exceed 1 cm for significant portions of each spiral (indicated with dots on the right side of each plot). The  $\lambda$ , or equivalently the median volume diameter,  $D_0 = \frac{3.67}{\lambda}$ , display vertical variability, with  $\lambda$  decreasing below about  $15 \text{ cm}^{-1}$  and  $D_0$  increasing above  $0.25 \text{ cm}$  (not plotted). The 2D probe images indicate that the  $D_{\max}$  increase downwards through aggregation.

[14] Of the nine spirals, the calculations indicate that five would have had dim bands. About 1/2 were found where  $-5 < T \leq 0^\circ\text{C}$  (Figure 4a). When the profiles derived from the PSD are smoothed to 100 m (300 m) in the vertical to simulate radar observations,  $Z_e$  at the top of the dim bands are  $7.6 \pm 2.0 \text{ dB}$  ( $7.3 \pm 2.3 \text{ dB}$ ) and  $18.9 \pm 3.6 \text{ dB}$  ( $18.4 \pm 4.1 \text{ dB}$ ) at 9.7 GHz (see also Figure 4b). Maximum diameters of the PSD need to exceed about 0.8 cm (Figure 4c). Presence of a dim band is likely for  $\lambda \leq 14 \text{ cm}^{-1}$  (Figure 4d). The mean IWC in the dim band is  $0.53 \pm 0.30$ .

[15] The primary factors responsible for the dimming can be studied conceptually by representing  $Z_e$  analytically:

$$Z_e [\text{mm}^6/\text{m}^3] = C_Z N_0 (10)^{12} \int_{D_l}^{D_h} \sigma(D) e^{-\lambda D} dD. \quad (1)$$

where  $C_Z = [\Lambda^4 \pi^{-5} (m x^2 + 2) / (m x^2 - 1)]$ ,  $\Lambda [\text{cm}]$  is the radar wavelength, and  $m x(\Lambda)$  is the complex refractive index of water. In equation (1), the bracketed term is taken to be  $4.91 \times 10^{-5} \text{ cm}^4$  (94 GHz) or  $0.333 \text{ cm}^4$  (9.7 GHz).  $N_0$  is in

$\text{cm}^{-4}$ . Integration is done numerically in diameter increments of  $20 \mu\text{m}$ ; interpolated values of  $\sigma$  from Figure 1 are used. We assume a minimum diameter  $D_l = 0.01 \text{ cm}$  and a maximum one  $D_h = 2 \text{ cm}$ . Also,

$$\text{IWC} [\text{g}/\text{m}^3] = a (10)^6 N_0 \int_{D_l}^{D_h} D^b e^{-\lambda D} dD. \quad (2)$$

For consistency, a constant value for IWC of  $0.5 \text{ g m}^{-3}$ , corresponding to a precipitation rate of about  $4 \text{ mm hr}^{-1}$ , is taken for all  $\lambda$ . This is achieved by choosing appropriate values of  $N_0$ .

[16] Figure 5a plots the model-derived  $Z_e$  with  $D$  for oblate particles. When  $\lambda = 30 \text{ cm}^{-1}$ , particles smaller than 0.08 cm contribute significantly to  $Z_e$ . The rate of increase in  $Z_e$  diminishes above 0.08 cm. Non-Rayleigh scattering has little effect on  $Z_e$  because relatively few large particles are present:  $Z_e$  at 9.7 GHz and 94 GHz are about the same. For  $\lambda = 8 \text{ cm}^{-1}$ , the contribution to  $Z_e$  from particles below 0.08 cm is much smaller than for  $\lambda = 30 \text{ cm}^{-1}$ . Although there are significant numbers of large particles, non-Rayleigh effects minimize their contribution to  $Z_e$  such that the total  $Z_e$  with low  $\lambda$  is below that for a large  $\lambda$ . For  $\lambda = 8 \text{ cm}^{-1}$ ,  $Z_e$  at 9.7 GHz is much larger than that for  $30 \text{ cm}^{-1}$ .

[17] As  $\lambda$  decreases from 30 to  $6 \text{ cm}^{-1}$ , the modeled  $Z_e$  for 94 GHz first increases, and then decreases when  $\lambda$  falls below  $15 \text{ cm}^{-1}$  (Figure 5b). At 9.7 GHz,  $Z_e$  increases with

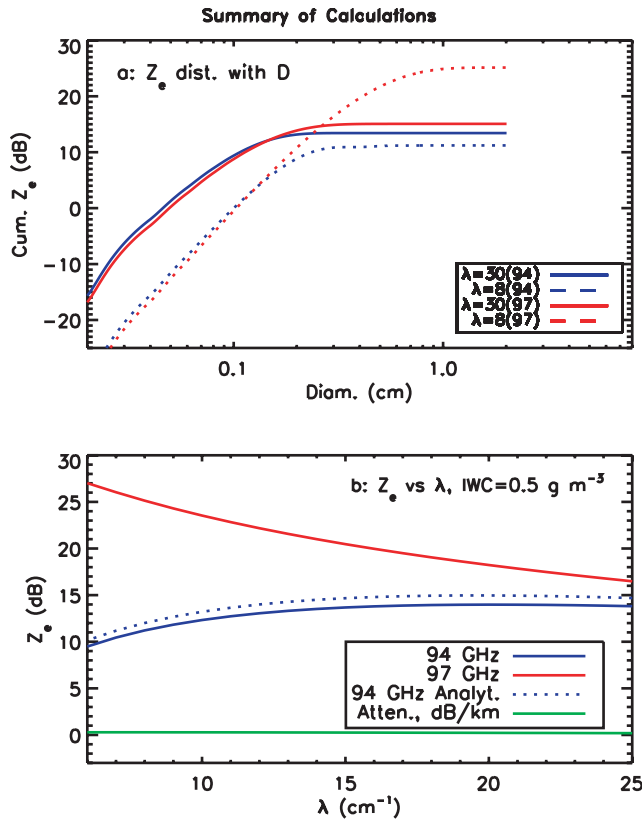


**Figure 5.** (a) Modeled cumulative  $Z_e$  with increasing diameter for two PSD slopes (curves) and (b) results for  $Z_e$  with  $6 \geq \lambda \geq 30 \text{ cm}^{-1}$ .

decreasing  $\lambda$ . These results mirror the calculations from the PSD during the Lagrangian spiral descents. The data indicate that the same IWC ( $0.5 \text{ g m}^{-3}$ ), can produce up to a 4 dB range in  $Z_e$ . Attenuation by snow (about  $0.2 \text{ dB/km}$  for all  $\lambda$ , see curve, Figure 5b) cannot explain these results. However, attenuation by liquid water if present (primarily from  $0$  to  $-5^\circ\text{C}$ ), could appreciably increase the dimming.

[18] A low bias in the IWC retrieved from  $Z_e$  measured by W band radar, such as CloudSat, could occur in the dimmed region. All else being equal (as with Figure 5b), a decrease of  $Z_e$  by 4 dB through dimming (Figures 4 and 5b) is equivalent to reducing  $N_0$  (Equation 1) by 0.4. As a result, the IWC would decrease by 60%. Ice sublimation in the dimmed zone (Figure 3c) could be interpreted erroneously as dimming and adds uncertainty IWC estimated from  $Z_e$ .

[19] The IWC through the dim band can be estimated from 94- and 9.7-GHz radar data together by rewriting Equation (1) as

$$Z_e = C_z N_0 (10)^{12} \left[ A \int_{0.01}^{D_h} D^B e^{-\lambda D} dD + \bar{\sigma} \int_{D_h}^{1.5} e^{-\lambda D} dD \right]. \quad (3)$$

where for 94 GHz  $D_l$  is  $0.2 \text{ cm}$  and  $D_h \approx 2 \text{ cm}$ . For 9.7 GHz, the Rayleigh regime predominates and the second term on the right hand side of Equation (3) is not used.  $A$  and  $B$  are used to represent the  $\sigma$  -  $D$  relationship for oblate ice in the Rayleigh regime (see fitted relationships given in Figure 2), and  $\bar{\sigma} = 0.00011 \text{ cm}^2$  for 94 GHz. Equation (3) produces

nearly the same  $Z_e$  as given by equation (1) if we use the same values of  $N_0$  and  $\lambda$  used to derive the dotted curve for 94 GHz in Figure 5b (see Figure 5b, “94 GHz analyt”). The value of  $\lambda$  is found from the dual wavelength ratio,  $\text{dWR} = Z_e(9.7 \text{ GHz}) - Z_e(94 \text{ GHz})$  in dB. Our coefficients give  $\lambda(\text{cm}^{-1}) = 35.1 - 23.8 \log_{10}(\text{dWR})$ . (Note that the dWR is invariant of the value of  $N_0$  and largely to the  $m(D)$  relationship and depends on the bracketed term in equation (3)). Equation (3) is then used to derive  $N_0$  and equation (2) the IWC. When only 94-GHz data are available with sufficient vertical resolution,  $\lambda \approx 14 \text{ cm}^{-1}$  is assigned at the height at which  $Z_e$  folds over—the top of the dim band. Given the measured value of  $Z_e$ ,  $N_0$  at this height can be derived from equation (3). The IWC can be assumed to remain constant through the dim band in lieu of additional information.

#### 4. Summary and Conclusions

[20] From two-wavelength radar observations taken from above an ice cloud layer during C-F, in-situ measurements of particle size distributions collected during nine Lagrangian spiral descents through ice cloud layers during KWAJEX and C-F, we can account for the properties of a 94-GHz dim band from non-Rayleigh scattering calculations for oblate ice particles, and a simple representation of exponential PSD. The results are consistent with ice particle aggregation, where the IWC may remain more or less constant in an ice cloud as height decreases from  $-5$  to  $0^\circ\text{C}$  whereas  $\lambda$  decreases, resulting in a PSD with more large particles and fewer small ones. The large particles introduce significant non-Rayleigh scattering at 94 GHz, often resulting in a decrease in  $Z_e$ . The  $\lambda$  in the dim band, predominantly  $<15 \text{ cm}^{-1}$ , can occur at any temperature, especially when convection is involved. Dimming is observed when  $Z_e$  reaches about 7 dB (94 GHz). We have observed what appears to be a few dB dimming in CloudSat profiles. This decrease in  $Z_e$  can introduce a low bias in the IWC retrieved from CloudSat. Methods to improve the IWC estimates from single (CloudSat) and two-wavelength data are proposed and could be modified if evaluations indicate that the radar backscatter coefficients or the mass dimensional relationships for aggregates used in this paper are in need of refinements.

[21] **Acknowledgments.** The author wishes to thank Gerald Heymsfield and Charlie Knight for providing data and for valuable discussions. Encouragement and support from the CloudSat Project Office and NASA are appreciated.

#### References

- Brown, P. R. A., and P. N. Francis (1995), Improved measurements of the ice water content in cirrus using a total-water probe, *J. Atmos. Oceanic Technol.*, *12*, 410–414.
- Heymsfield, A. J., A. Bansemer, P. R. Field, S. L. Durden, J. Stith, J. E. Dye, W. Hall, and T. Grainger (2002), Observations and parameterizations of particle size distributions in deep tropical cirrus and stratiform precipitating clouds: Results from in-situ observations in TRMM field campaigns, *J. Atmos. Sci.*, *59*, 3457–3491.
- Heymsfield, A. J., G.-J. van Zadelhoff, D. P. Donovan, F. Fabry, R. J. Hogan, and A. J. Illingworth (2007), Refinements to ice particle mass dimensional and terminal velocity relationships for ice clouds. Part II: Evaluation and parameterizations of ensemble ice particle sedimentation velocities, *J. Atmos. Sci.*, *64*, 1068–1088.
- Kollias, P., and B. Albrecht (2005), Why the melting layer radar reflectivity is not bright at 94 GHz, *Geophys. Res. Lett.*, *32*, L24818, doi:10.1029/2005GL024074.

- Lhermitte, R. (1988), Observation of rain at vertical incidence with a 94 GHz Doppler radar: An insight on Mie scattering, *Geophys. Res. Lett.*, *15*, 1125–1128.
- Matrosov, S. Y., A. J. Heymsfield, and Z. Wang (2005), Dual-frequency radar ratio of nonspherical atmospheric hydrometeors, *Geophys. Res. Lett.*, *32*, L13816, doi:10.1029/2005GL023210.
- Sassen, K., J. R. Campbell, J. Zhu, P. Kollias, M. Shupe, and C. Williams (2005), Lidar and triple-wavelength Doppler radar measurements of the melting layer: A revised model for dark and bright band phenomena, *J. Appl. Meteorol.*, *44*, 301–312.
- Sassen, K., S. Matrosov, and J. Campbell (2007), CloudSat spaceborne 94 GHz radar bright bands in the melting layer: An attenuation-driven upside-down lidar analog, *Geophys. Res. Lett.*, *34*, L16818, doi:10.1029/2007GL030291.
- Stephens, G. L., et al. (2002), The CloudSat mission and the EOS constellation: A new dimension of space-based observations of clouds and precipitation, *Bull. Am. Meteorol. Soc.*, *83*, 1771–1790.
- Tian, L., G. M. Heymsfield, L. Li, and R. C. Srivastava (2007), Properties of light stratiform rain derived from 10- and 94-GHz airborne Doppler radars measurements, *J. Geophys. Res.*, *112*, D11211, doi:10.1029/2006JD008144.
- 
- A. Bansemmer and A. J. Heymsfield, NCAR, 3450 Mitchell Lane, Boulder CO 80301 USA. (heyms1@ucar.edu)
- S. Matrosov, Environmental Technology Laboratory, NOAA, 325 Broadway, Boulder, CO 80303, USA.
- L. Tian, NASA Goddard Space Flight Center, Greenbelt, MD 20771-0001, USA.